RSC Advances

PAPER

View Article Online
View Journal | View Issue

Cite this: *RSC Adv.*, 2020, **10**, 41967

Synthesis and structures of divalent Co, Ni, Zn and Cd complexes of mixed dichalcogen and dipnictogen ligands with corrosion inhibition properties: experimental and computational studies†

Tunde L. Yusuf,[a] Taiwo W. Quadri,[b] Gideon F. Tolufashe,[c] Lukman O. Olasunkanmi,[bd] Eno E. Ebenso[be] and Werner E. van Zyl*[a]

The structural and corrosion inhibition properties of four different transition-metal complexes of heteroleptic S-donor atom dithiophosphonate and N-donor atom phenanthroline ligands are reported. Full structural characterization of the Co, Ni, Zn and Cd complexes was achieved with the aid of single-crystal X-ray crystallography. Structural elucidation revealed the formation of a 4-coordinate Zn(II) complex, and 6-coordinate Ni(II) and Cd(II), as well as a novel dithiophosphonato Co(II) complex. The ability of the complexes with this ligand type to act as inhibitors of mild steel corrosion in 1 M HCl solution is reported for the first time. Corrosion inhibition potentials of the complexes were assessed using potentiodynamic polarization, electrochemical impedance spectroscopy (EIS), and density functional theory (DFT). The open circuit potential (OCP) time profile showed the system achieved a steady-state potential before the first 600 s after submerging the working electrode in the corrosive medium. The studied metal complexes are good inhibitors of mild steel corrosion in 1 M HCl and were found to retard the corrosion rate by forming an adsorbed pseudocapacitive film on the steel surface. The order of inhibition efficiencies was in the order Ni (94.14%) > Cd (92.28%) > Zn (91.14%) > Co (72.53%).

Received 10th September 2020
Accepted 8th November 2020

DOI: 10.1039/d0ra07770d

rsc.li/rsc-advances

1. Introduction

Mild steel is one of the most used steels due to its relative low-cost and good mechanical strength.[1–3] Mild steel is widely used in the petroleum industry as transport pipes for oil in petroleum production and refining, chemical processing industries, engineering materials in transportation, pipeline industries, mining and marine applications, nuclear power plants, construction and metal processing equipment.[4,5] Mild steel is, however, susceptible to corrosion, especially in acidic conditions and can readily be exposed to acid during acid cleaning, acid pickling and acid descaling, which are famous industrial procedures.[6–10] The use of corrosion inhibitors in different media has become an efficient and common way of protecting metallic surfaces from corrosion[11–13] because it is easy to apply and relatively inexpensive.[4,13,14]

Organic compounds with heteroatoms like O, S, P and N often display potentials to inhibit metal corrosion in different electrolytic media.[15,16] The inhibition properties of these classes of compounds are attributed to their strong polarizability and low electronegativity. The presence of heteroatoms in corrosion inhibitors facilitates transfer of electrons to empty atomic orbitals in the metal, thereby promotes adsorption of the inhibitor molecule on the metallic surface.[17] Reports showed that nitrogen-containing organic compounds are excellent anti-corrosion agents for metals in hydrochloric acid solution, while sulfur-containing compounds have the tendency to perform better in inhibiting metal corrosion in sulphuric acid solution.[18] Furthermore, compounds containing N- and S- atoms usually exhibit substantial inhibition potentials in both hydrochloric and sulphuric acid solutions.[19] The efficiency of inhibitors with different heteroatoms usually increases with decreasing

[a]*School of Chemistry and Physics, University of KwaZulu-Natal, Westville Campus, Chiltern Hills, Private Bag X54001, Durban, 4000, South Africa. E-mail: vanzylw@ukzn.ac.za; Tel: +27 31 260 3188*

[b]*Department of Chemistry, School of Physical and Chemical Sciences, Materials Science Innovation and Modelling (MaSIM) Research Focus Area, Faculty of Natural and Agricultural Sciences, North-West University (Mafikeng Campus), Private Bag X2046, Mmabatho 2735, South Africa*

[c]*Department of Chemistry and Biochemistry, Faculty of Sciences, University of Porto, 4169-007 Porto, Portugal*

[d]*Department of Chemistry, Faculty of Science, Obafemi Awolowo University, Ile-Ife 220005, Nigeria*

[e]*Institute for Nanotechnology and Water Sustainability, College of Science, Engineering and Technology, University of South Africa, Johannesburg, South Africa*

† Electronic supplementary information (ESI) available. CCDC 2008849–2008851, 2008799, 2008800. For ESI and crystallographic data in CIF or other electronic format see DOI: 10.1039/d0ra07770d

electronegativity, such that the trend of inhibition efficiencies with respect to heteroatoms is in the order O < N < S < P.[20]

Metal complexes have also been reported to show excellent corrosion inhibition activities.[21,22] The interaction of transition metal complexes with mild steel is significantly affected by the reactivity and nature of the ligand and the standard electrode potential of the metal cation.[22] The standard electrode potential of divalent cations considered in the present study follows the order: Ni(II)/Ni(−0.23 V) > Co(II)/Co (−0.277 V) > Cd(II)/Cd (−0.40 V) > Zn(II)/Zn (−0.76 V)[23] and the incorporation of metal into a heteroatom-rich ligand should improve its corrosion inhibition potentials.

Electrochemical techniques like potentiodynamic polarization (PDP) and electrochemical impedance spectroscopy (EIS) are powerful techniques that are widely used to research electrochemical corrosion. Inhibition efficiencies of corrosion inhibitors, and organic and inorganic coatings are usually estimated from PDP and EIS measurements.[24–27] Computational studies are often used to provide corroborative explanations to the experimental findings.[28] Quantum chemical calculations are employed to investigate possible correlations between molecular quantum chemical descriptors and specific reactivities of a molecular system, including adsorption behaviour, which translates to corrosion inhibition[14,29–31]

Inspired by the application of zinc dialkyldithiophosphates (ZDDPs) as an antioxidant in the oil industry,[32] we synthesized and characterized four new transition-metal complexes (Co^{2+}, Ni^{2+}, Zn^{2+} and Cd^{2+}) of dithiophosphonate and N-donor (2,2-bipyridine, 1,10-phenanthroline) ligands, and assessed their corrosion inhibition properties for mild steel in 1 M HCl. Additionally, single crystal X-ray crystallography revealed new structures and were further supported by elemental analysis, magnetic susceptibility measurements, multi-nuclear magnetic resonance, Fourier transform infrared and electronic spectroscopies, and mass spectrometry.

2. Experimental

2.1 Materials and methods

All reactions were performed using standard Schlenk line techniques under a nitrogen atmosphere. All chemicals were purchased from commercial sources. Tetrahydrofuran (THF) and dichloromethane (DCM) was dried using Innovative Technology PURE-SOLV solvent purification system, USA. NMR spectra were recorded on a Bruker AV-400 instrument operating at 400 MHz while ^{1}H and ^{31}P was recorded at 162 MHz. For the ^{1}H residual solvent proton a standard reference was used (δ, ppm, $CDCl_3$, 7.26). For ^{31}P NMR, H_3PO_4 (85%) was used as an external reference. The melting points were measured on an Electrothermal 9100 melting point apparatus and are uncorrected. The electronic absorption spectra were recorded on a Shimadzu UV-3600 UV-VIS-NIR spectrophotometer using quartz cuvettes having a path length of 1 cm in the range 200–400 nm for UV and 400–900 nm visible regions. Electrospray ionization mass spectra (ESI-MS) for the complexes were recorded using a Waters Micromass LCT Premier TOF-MS. The LC/MS spectra of the ligand and some complexes were obtained from Shimadzu LCMS-2020 using ESI methods. The molar conductance of 10^{-3} M complexes in DMSO solutions was obtained at room temperature on an Edge HI2003 conductivity meter.

2.2 Synthesis of ligand

2.2.1 Synthesis of [NH_4][S_2P{1,4-C_6H_4OMe}{$OCH(CH_3)_2$}] (L1). An oven dried Schlenk flask was charged with Lawesson's reagent (1.0 g, 2.47 mmol) and iso-propanol (0.4 mL, 4.94 mmol) in a dry THF mixture (30 mL) and stirred for 30 minutes until the solution was clear. The solution was cooled to 0 °C in an ice-bath and anhydrous NH_3 gas was bubbled into the clear solution to afford a white precipitate. The mixture was concentrated and further stirred in dry hexane (30 mL). A colourless free flowing powder was obtained upon removal of the solvent under reduced pressure. Yield: 1.31 g (96%) melting point: 112–114 °C ^{1}H NMR (400 MHz, DMSO-d_6) δ 7.91 (dd, J = 12.8, 8.6 Hz, 2H, Ar–H), 7.24 (bs, 4H, NH_4), 6.84 (dd, J = 8.8, 2.4 Hz, 2H, Ar–H), 4.59–4.40 (m, 1H, OCH), 3.76 (s, 3H, Ar–OCH_3), 1.04 (d, J = 6.2 Hz, 6H, CH_3). ^{13}C NMR (101 MHz, DMSO-d_6) δ 160.01, 139.21, 138.11, 131.96, 131.83, 113.57, 112.39, 112.26, 66.42, 66.36, 55.51, 24.66, 24.63. LC/MS MS: m/z 263 ([M + 2H]$^+$) IR(ATR, cm^{-1}) 2838(s), 1594(s), 1571(s), 1496(s), 1464(s), 1439(s), 1406(s), 1303(s), 1291(s). 1241(s), 1217(s), 1178(s), 1045(s), 1019(s), 925(s), 862(s), 824(s).

2.2.2 Synthesis of [NH_4][S_2P{1,4-C_6H_4OMe}{$OCH_2CH_2CH_3$}] (L2). The ligand was prepared similar to ligand **L1** above. Yield: 1.35 g (98%) melting point: 118–119 °C. ^{1}H NMR (400 MHz, DMSO-d_6) δ 7.90 (dd, J = 12.9, 8.6 Hz, 2H, Ar–H), 6.86 (dd, J = 8.8, 2.4 Hz, 2H, Ar–H), 6.81 (bs, 4H, NH_4), 3.75 (s, 3H, Ar–OCH_3), 3.64–3.56 (m, 2H, OCH_2), 1.46 (h, J = 7.2 Hz, 2H, CH_2), 0.79 (t, J = 7.4 Hz, 3H, CH_3). ^{13}C NMR (101 MHz, DMSO-d_6) δ 160.20, 160.17, 138.12, 137.02, 131.91, 131.78, 112.62, 112.48, 64.49, 64.42, 55.58, 23.87, 23.78, 10.95. LC/MS MS: m/z 263 ([M + 2H]$^+$), 523 (2[M]$^+$). IR(ATR, cm^{-1}) 2836(s), 1586(s), 1570(s), 1491(s), 1458(s), 1440(s), 1313(s), 1295(s). 1238(s), 1219(s), 1179(s), 1046(s), 1028(s), 924(s), 860(s), 826(s).

2.3 Synthesis of metal complexes

2.3.1 Synthesis of [Co{S_2P(1,4-C_6H_4OMe)($OCH(CH_3)_2$)}$_2${phen}] (1). A mixture of $CoCl_2\cdot 6H_2O$ (238 mg, 1 mmol) and **L1** (559 mg, 2 mmol) in ethanol solution (25 mL) was stirred in a beaker for 25 minutes. To the resulting blue mixture was added 1,10-phenanthroline monohydrate (198 mg, 1 mmol) and stirred for 1 hour. The resulting brown precipitate was filtered and washed with water/ethanol mixture (50 : 50). Single crystals suitable for X-ray diffraction were obtained by vapour diffusion of hexane into DCM. Yield: 640 mg (84%). Melting point: 186–188 °C LC-MS(m/z) (cal.) 761(761) for ([M]$^+$; 500 (500) ([M-{S_2P(4-$C_6H_4OCH_3$)(OC_3H_7)}]$^+$. μ_{eff} = 4.82 B.M. Anal. calc. for C, 50.46; H, 4.76; N, 3.68, found: C, 49.98; H, 4.91; N, 3.78.

2.3.2 Synthesis of [Ni{S_2P(1,4-C_6H_4OMe)($OCH_2CH_2CH_3$)}$_2${phen}] (2). To a stirring methanol solution (30 mL) of **L2** (559 mg, 2 mmol) was added a solution of $NiCl_2\cdot 6H_2O$ (238 mg, 1 mmol) in ethanol in a dropwise manner. To the resulting violet solution was added 1,10-phenanthroline (198 mg, 1

mmol) with constant stirring resulting in a brown coloured precipitate. The precipitate was filtered *in vacuo* and washed with methanol and water (50 : 50)% to afford a light green powder. Single crystals suitable for X-ray diffraction were obtained as light green blocks from vapour diffusion of hexane into a concentrated DCM solution. Yield: 568 mg (75%). Melting point: 147–149 °C. μ_{eff} = 2.83 B.M. Anal. calc. for $C_{32}H_{36}N_2NiO_4P_2S_4$: C, 50.47; H, 4.77; N, 3.68, found: C, 50.34; H, 4.95; N, 3.54.

2.3.3 Synthesis of [Zn{$S_2P(1,4\text{-}C_6H_4OMe)(OCH_2CH_2CH_3)$}{phen}] (3). An ethanolic solution of $ZnNO_3 \cdot 6H_2O$ (297 mg, 1 mmol) was added to a stirring solution of **L2** (559 mg, 2 mmol) in ethanol. The solution was stirred for 20 min and 1,10-phenanthroline monohydrate (198 mg, 1 mmol) was added to the mixture and further allowed to stir for 1 hour, the resulting white precipitated was filtered and washed with ethanol/water. Recrystallization from hexane layered over DCM yielded colourless block crystals in two weeks. Yield: 607 mg (79%). Melting point 211 °C (dec.). ^{13}C NMR (151 MHz, chloroform-*d*) δ 161.50, 149.75, 140.79, 139.08, 131.92, 131.82, 128.85, 126.83, 125.26, 113.06, 112.96, 66.80, 55.26, 23.61, 23.55, 10.30. ^{31}P NMR (243 MHz, chloroform-*d*) δ 103.50, 100.21. ESI-MS(*m*/*z*) (cal.) 505.0329 (505.0152) for ([M-{$S_2P(4\text{-}C_6H_4OMe)(OCH_2CH_2CH_3)$}]$^+$, 100%). Anal. calc. for $C_{32}H_{36}N_2O_4P_2S_4Zn$: C, 50.03; H, 4.72; N, 3.65, found: C, 49.92; H, 4.80; N, 3.78 IR(ATR, cm^{-1}) 2970(s), 2939(s), 2882(s), 1623(s), 1594(s), 1570(s), 1516(s),1499(s), 1461(s),1439(s),1423(s), 1373(s), 1321(s), 1294(s), 1183(s).

2.3.4 Synthesis of [Cd{$S_2P(1,4\text{-}C_6H_4OMe)(OCH_2CH_2CH_3)$}$_2${phen}] (4). In a beaker, a $Cd(NO_3)_2 \cdot 4H_2O$ (308 mg, 1 mmol) methanol solution (20 mL) was added dropwise to a stirring solution of 1,10-phenanthroline (198 mg, 1 mmol) and **L2** (559 mg, 2 mmol) in 40 mL methanol. A white precipitate immediately formed and was further stirred for 1 hour at room temperature. The precipitate was collected by filtration and washed with MeOH : H_2O (50 : 50) solvent. The resulting colourless solid was dried in air. Slow evaporation from acetone yielded colourless crystals suitable for X-ray diffraction measurement. Yield: 717 mg (88%). Melting point: 256 °C (dec.). ^{1}H NMR (400 MHz, chloroform-*d*) δ 9.52 (s, 2H), 8.37 (dd, J = 8.2, 1.6 Hz, 2H), 7.90–7.80 (m, 6H), 7.76 (dd, J = 8.2, 4.7 Hz, 2H), 6.76 (dd, J = 8.8, 2.9 Hz, 4H), 4.13 (dt, J = 9.1, 6.7 Hz, 4H), 3.72 (s, 6H), 1.66 (dt, J = 14.2, 7.1 Hz, 4H), 0.86 (t, J = 7.4 Hz, 6H). ^{13}C NMR (101 MHz, chloroform-*d*) δ 161.51, 149.74, 138.26, 131.84, 131.70, 129.09, 126.89, 124.68, 113.29, 113.13, 66.81, 55.31, 23.71, 23.63, 10.40 anal. calc. for $C_{32}H_{36}CdN_2O_4P_2S_4$: C, 47.15; H, 4.45; N, 3.44; S, 15.73, found: C, 47.01; H, 4.56; N, 3.30; S, 15.13.

2.4 X-ray crystallography

Crystal evaluation and data collection of **1–4** were done on a Bruker Smart APEXII diffractometer equipped with an Oxford Cryostream low-temperature apparatus operating at 100 K, with Mo-Kα radiation (I = 0.71073 Å). Reflections were collected at different starting angles and the APEXII program suite was used to index the reflections.[33] Data reduction was performed using SAINT[34] software, and the scaling and absorption corrections were applied using the SADABS[35] multi-scan technique. The structure was solved by direct methods using the SHELXS program and refined using SHELXL program.[36] Graphics of the crystal structures were drawn using Mercury software.[37] Non-hydrogen atoms were first refined isotropically and then by anisotropic refinement with the full-matrix least square method based on F^2 using SHELXL. All hydrogen atoms were positioned geometrically, allowed to ride on their parent atoms and refined isotropically.

2.5 Electrochemical measurements

To explore the effect of the synthesized complexes on the corrosion of mild steel in 1 M HCl, impedance and polarization tests were conducted in the absence and presence of the synthesized complexes. The mild steel sheets purchased from commercial supplier with a chemical composition of (in wt%): Fe (99.621), C(0.076), P (0.012), Cr (0.050), Al (0.023), Si (0.026), Mn (0.192) were cut into 1 cm × 1 cm dimension and embedded in epoxy resin leaving an exposed area of 1 cm^2. Mechanical abrasion of the exposed surface was done with the aid of a Struers LaboPol-1 machine to eliminate traces of epoxy resin. Thereafter different grade emery papers ranging from 600 to 1200 were used to polish the exposed surface to eliminate surface rusts and scales. The steel surface was thereafter washed thoroughly with distilled water, degreased with acetone and dried at room temperature. The aggressive electrolytic solution of 1 M HCl was prepared by dilution of 32% HCl. The complexes were first dissolved in a small volume of DMSO (10% of total solvent volume) to ensure uniform dissolution without turbidity. Stock solutions of the complexes were subsequently prepared in 1 M HCl. Preliminary checks on the performance of the complexes as corrosion inhibitors suggested that a concentration of 100 ppm is optimum and the inhibition efficiencies were thus tested at 100 ppm.

Electrochemical studies were conducted on the AUTOLAB (model 302N) potentiostat/galvanostat coupled with a three-electrode assemblage driven by Nova 1.10.1.9 software. A typical electrochemical system setup has the polished mild steel as the working electrode, Ag/AgCl, 3 M KCl as the reference electrode and a platinum rod as the counter electrode which are all submerged in the electrolyte. A waiting time of 1800 s was allowed for the mild steel in the electrolyte to corrode freely without applying external potential or current in order to obtain a stable open circuit potential (OCP). After the steady-state potential was achieved, EIS tests were conducted at the OCP by evaluating the frequency response of the system in the range of 100 kHz to 0.01 Hz with an amplitude of 10 mV. These EIS measurement settings are considered to be wide enough to sufficiently reveal the resistive and capacitive behaviour of the electrochemical system, and also comply with the recommended ASTM practice G106-89.[38] All electrochemical tests conducted were done under aerated unstirred conditions at 303 ± 1 K. Values of charge transfer resistance were generated from the obtained impedance spectra. Percentage inhibition efficiencies (η_{EIS}) of the studied compounds were calculated from the measured charge transfer resistance (R_{ct}) values using the following equation:[39]

$$\eta_{EIS} = \frac{R_{ct} - R_{ct}^{0}}{R_{ct}} \times 100$$

where R_{ct} and R_{ct}^{0} represent the values of the charge transfer parameters with and without the inhibitors, respectively.

Polarization measurements were performed by sweeping the potential from −250 to +250 mV with respect to the OCP at a constant scan rate of 1 mV s^{-1}. The measurement parameters are chosen within the recommended limits in the ASTM F 2129 standard practice.[40] Corrosion current densities (i_{corr}) were obtained by extrapolating the linear segments of the anodic and cathodic Tafel slopes to corrosion potential. The percentage inhibition efficiency (η_{PDP}) was calculated from the obtained values of i_{corr} using the equation:[41]

$$\eta_{PDP} = \frac{i_{corr}^{0} - i_{corr}}{i_{corr}^{0}} \times 100$$

where i_{corr} and i_{corr}^{0} represent the corrosion current densities with and without the studied inhibitors, respectively.

In order to measure the linear polarization resistance, a potential range of ±10 mV relative to OCP was applied to the system and current response was monitored at a scan rate of 0.125 mV s^{-1}. Values of polarization resistance (R_p) for the blank and inhibited system were obtained from this method and the percentage inhibition efficiency was calculated thus:[42]

$$\eta_{LPR} = \frac{R_p - R_p^{0}}{R_p} \times 100$$

where R_p and R_p^{0} represent the polarization resistances in the presence and absence of the studied inhibitors, respectively.

2.6 Computational studies

The quantum chemical calculations for the inhibitors were performed in the gas phase using density functional theory

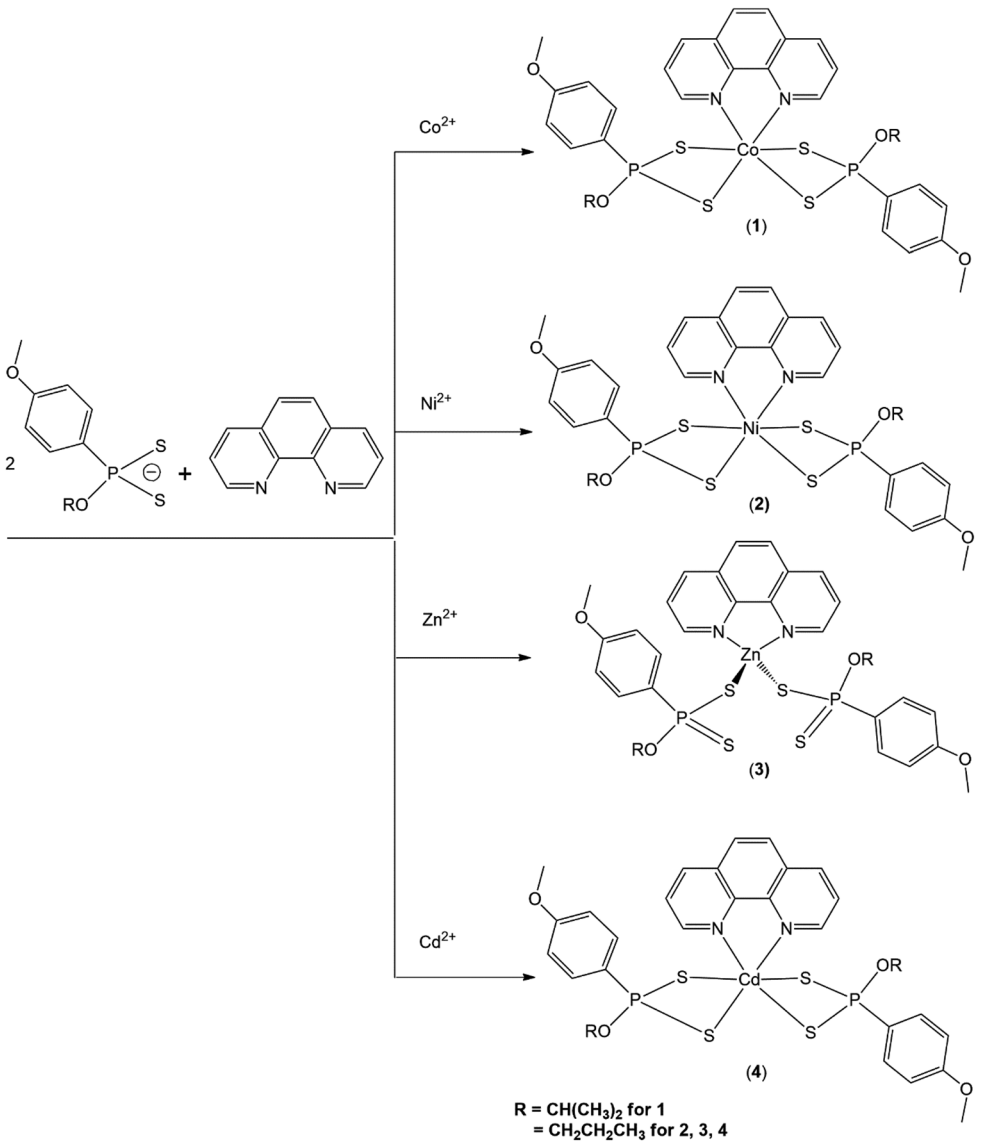

Scheme 1 Summary of the synthesis methodology for the preparation of complexes 1–4.

Table 1 Crystallographic data and structure refinement for **1a**, **1b**, **2**, **3** and **4**

Compound	**1a**	**1b**	**2**	**3**	**4**
Empirical formula	$C_{32}H_{36}CoN_2O_4P_2S_4$	$C_{32}H_{36}CoN_2O_4P_2S_4$	$C_{32}H_{36}N_2NiO_4P_2S_4$	$C_{32}H_{36}N_2O_4P_2S_4Zn$	$C_{32}H_{36}CdN_2O_4P_2S_4$
Formula weight	761.74	761.74	761.52	768.18	815.21
Temperature/K	100(2)	150(2)	100(2)	100(2)	100
Crystal system	Monoclinic	Triclinic	Triclinic	Triclinic	Monoclinic
Space group	$C2/c$	$P\bar{1}$	$P\bar{1}$	$P\bar{1}$	$C2/c$
a/Å	22.9770(4)	10.8831(2)	10.8316(6)	10.02980(10)	49.6546(10)
b/Å	10.7463(2)	12.4185(2)	13.2433(8)	12.6887(2)	11.0919(2)
c/Å	15.6178(3)	14.1718(3)	14.1413(9)	14.1918(2)	34.7070(7)
α/°	90	91.5350(10)	65.148(3)	87.0380(10)	90
β/°	113.0040(10)	97.5390(10)	89.961(3)	78.8780(10)	112.9760(10)
γ/°	90	109.8070(10)	71.017(3)	73.5350(10)	90
Volume/Å^3	3549.65(12)	1781.23(6)	1718.55(18)	1699.52(4)	17 598.9(6)
Z	4	2	2	2	20
ρ_{calc} g cm^{-3}	1.425	1.420	1.472	1.501	1.538
μ/mm^{-1}	0.847	0.844	0.940	1.102	0.987
F(000)	1580.0	790.0	792.0	796.0	8320.0
Crystal size/mm^3	0.41 × 0.32 × 0.23	0.33 × 0.22 × 0.12	0.24 × 0.21 × 0.16	0.42 × 0.22 × 0.191	0.3 × 0.24 × 0.21
Radiation	MoKα (λ = 0.71073)	MoKα (λ = 0.71073)	MoKα (λ = 0.71073)	MoKα (λ = 0.71073)	MoKα (λ = 0.71073)
2Θ range for data collection/°	3.852 to 57.042	3.496 to 54.392	3.214 to 52.448	3.348 to 54.81	1.782 to 56.772
Index ranges	$-30 \le h \le 27$, $-14 \le k \le 14$, $-20 \le l \le 20$	$-13 \le h \le 13$, $-15 \le k \le 15$, $-18 \le l \le 18$	$-13 \le h \le 13$, $-16 \le k \le 16$, $-16 \le l \le 17$		$-66 \le h \le 65$, $-14 \le k \le 14$, $-46 \le l \le 46$
Reflections collected	23 063	20 669	23 029	20 706	139572
Independent reflections	4403 [R_{int} = 0.0168, R_{sigma} = 0.0131]	7650 [R_{int} = 0.0182, R_{sigma} = 0.0227]	6684 [R_{int} = 0.0234, R_{sigma} = 0.0245]	7546 [R_{int} = 0.0117, R_{sigma} = 0.0137]	21 937 [R_{int} = 0.0337, R_{sigma} = 0.0247]
Data/restraints/parameters	4403/0/207	7650/1/412	6684/0/410	7546/0/431	21 937/0/1024
Goodness-of-fit on F^2	1.050	1.040	1.112	1.048	1.188
Final R indexes [$I \ge 2\sigma$ (I)]	R_1 = 0.0226, wR_2 = 0.0614	R_1 = 0.0266, wR_2 = 0.0621	R_1 = 0.0562, wR_2 = 0.1379	R_1 = 0.0297, wR_2 = 0.0800	R_1 = 0.0417, wR_2 = 0.0891
Final R indexes [all data]	R_1 = 0.0247, wR_2 = 0.0629	R_1 = 0.0344, wR_2 = 0.0664	R_1 = 0.0611, wR_2 = 0.1413	R_1 = 0.0323, wR_2 = 0.0820	R_1 = 0.0525, wR_2 = 0.0930
Largest diff. peak/hole/e Å^{-3}	0.51/−0.23	0.34/−0.27	1.55/−0.85		1.80/−1.44

(DFT). The density functional theory (DFT) calculations were executed applying the hybrid BP86 exchange-correlation functional with the Def2TZVP[43] basis set for geometry optimization of the structures using Gaussian'16 program package.[44] The synergy between the BP86 functional and the Def2TZVP basis set have been reported.[43,45] However, for the nickel complex, B3LYP[46] functional with LANL2DZ was utilized and have been previously reported for Ni complexes.[47] Optimizations to a local minimum for all structures using the Berny algorithm[48] was confirmed with no negative imaginary frequencies. This indicates that the structure geometry was obtained with a stationary point on the potential surface. The highest occupied molecular orbital (HOMO) and lowest unoccupied molecular orbital (LUMO) energies were obtained for all the metal complexes. The difference between the energy of the LUMO and HOMO results in the energy gap (ΔE). Other reactivity descriptors were derived such as the ionization potential (I) and electron affinity (A), absolute hardness (η), softness (S), electrophilicity index (ω) and absolute electronegativity (χ) of the complexes based on Koopman's theorem.[49] These descriptors are derived as follows:

$$\Delta E = E_{\mathrm{LUMO}} - E_{\mathrm{HOMO}}$$

$$I = -E_{\mathrm{HOMO}}$$

$$A = -E_{\mathrm{LUMO}}$$

$$\eta = \frac{E_{\mathrm{LUMO}} - E_{\mathrm{HOMO}}}{2}$$

$$S = \frac{1}{2\eta}$$

$$\chi = \frac{E_{\mathrm{LUMO}} + E_{\mathrm{HOMO}}}{2}$$

$$\omega = \frac{\mu 2}{2\eta}$$

3. Results and discussion

3.1 Synthesis of complexes

The methodology for the synthesis of complexes **1–4** are summarized in Scheme 1. The molecular structure for any homoleptic cobalt(II) dithiophosphonato complex has to date eluded isolation and the formation of such complexes are thus performed by the introduction of N-donor ligands such as 1,10-phenanthroline and 2,2-bipyridine. The cobalt(II) complex **1** was isolated from a mixture of $CoCl_2 \cdot 6H_2O$ precursor, ammonium dithiophosphonate ligand (**L1**) and 1,10-phenanthroline in 1 : 2 : 1 molar ratio. Complex **1** is soluble in chlorinated solvents, acetone, and THF but insoluble in *n*-hexane and water. The nickel(II) complex **2** was synthesized from the reaction between $NiCl_2 \cdot 6H_2O$, 1,10-phenanthroline and **L2**, in a stoichiometric ratio of 1 : 1 : 2. The complex was isolated in high yield as an air and moisture stable powder. Complex **2** was soluble in DCM, chloroform, acetone and THF but insoluble in alcohols, water, ether and *n*-hexane. The zinc(II) complex **3** was synthesized in high yield as air and moisture stable white solid by the reaction between $Zn(NO_3)_2 \cdot 6H_2O$, 1,10-phenanthroline and **L2** in a stoichiometric ratio of 1 : 1 : 2 at room temperature. The complex is soluble in DCM, acetone, chloroform and THF but insoluble in alcohols, ether, *n*-hexane and water. The low molar conductance values of 10^{-3} M solutions of the complexes in DMSO at room temperature (8.94–22.60 Ω^{-1} cm^2 mol^{-1}) indicate that the complexes are non-electrolytes.[50] Complex **3** is diamagnetic and the ^{1}H, ^{13}C and ^{31}P NMR data were generated from $CDCl_3$ solution, whilst FT-IR data was obtained in the solid-state. A zinc(II) complex of dithiophosphate with 4,4-bipyridine was reported by Glinskaya *et al.*, adopting a distorted

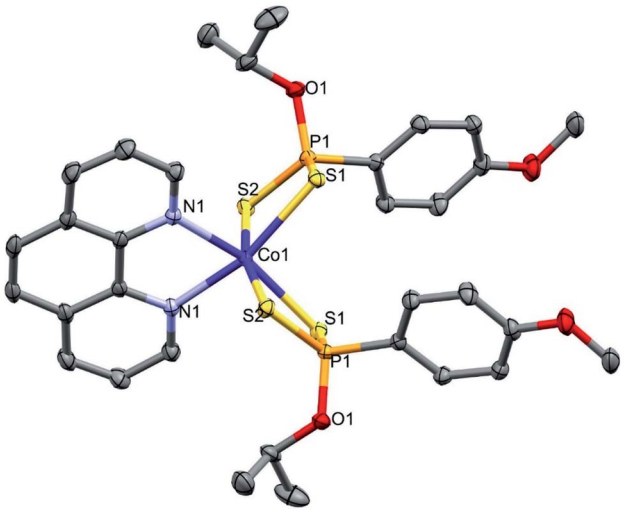

Fig. 1 Molecular structure for one of the polymorphs of **1** with thermal ellipsoids drawn at 50% probability. Hydrogen atoms omitted for clarity.

Table 2 Selected bond lengths (Å) and angles (°) for **1a** and **1b**, **2** with the estimated standard deviation (e.s.d.) in parentheses

Complex	1a	1b	Complex	2
Co1–S1	2.5063(3)	2.5496(5)	Ni1–S1	2.3217(5)
Co1–S2	2.5061(3)	2.4574(5)	Ni1–S2	2.3034(5)
Co1–N1	2.1526(10)	2.1486(13)	Ni1–N1	2.1247(16)
Co1–N2	2.1526(9)	2.1473(14)	Ni1–N2	2.0588(15)
S1–P1	1.9992(4)	1.9931(6)	S1–P1	2.0309(8)
S2–P2	1.9902(4)	1.9898(6)	S2–P2	2.0287(6)
P1–O1	1.6027(9)	1.6006(12)	P1–O1	1.6013(16)
P2–C13	1.7928(12)	1.8038(17)	P2–O2	1.6125(14)
O1–C1	1.4580(14)	1.451(2)	P2–C13	1.800(2)
N3–C11	1.3602(14)	1.362(2)	O1–C3	1.443(3)
S1–Co1–S2	96–542(14)	99.263(16)	S1–Ni1–S2	81.540(15)
N1–Co–S1	94.63(3)	93.15(4)	N1–Ni–S1	93.33(4)
N1–Co–N2	76.73(5)	76.81(5)	N1–Ni–N2	80.18(5)

tetrahedron geometry,[51] but the present study reports a mononuclear zinc(II) complex for a dithiophosphonate ligand with a 4-coordinate geometry for the first time. The cadmium(II) complex, **4** was isolated as colourless solid from a mixture of $Cd(NO_3)_2 \cdot 4H_2O$ salt, ligand **L2** and 1,10-phenanthroline in alcohol in a 1 : 2 : 1 stoichiometric ratio. The complex is soluble in DCM, chloroform and acetone but insoluble in water, *n*-hexane and alcohols.

3.2 NMR spectroscopy

The NMR spectra for complexes **1** and **2** were not recorded due to their paramagnetic nature. Magnetic susceptibility measurements gave magnetic moments of 4.82 and 2.83 B.M for **1** and **2** respectively, indicative of a high spin complexes with four unpaired electrons for **1** and two unpaired electrons for **2**, both of which are paramagnetic with octahedral geometries. The NMR data for complex **3** are presented in the experimental section. The methoxy protons for **3** were observed at 3.75 ppm as singlet peaks and the terminal methyl peak in the (OR) fragment was observed at 0.79 ppm. The other propoxyl protons in **3** were observed at 3.64 ppm for OCH_2– and 1.46 ppm for $–OCH_2\mathbf{CH_2}CH_3$, with the aromatic protons, observed 9.30–6.56 ppm. The ^{1}H NMR spectrum for **4** showed peaks associated with 1,10-phenanthroline in the range of 7.83–9.48 ppm; while the singlet peak at 3.72 ppm is diagnostic of OCH_3 of the anisyl fragment of Lawesson's reagent.

3.3 X-ray crystallography

The X-ray crystal structure of **1** consisted of discrete mononuclear molecular units. The crystallographic and structure

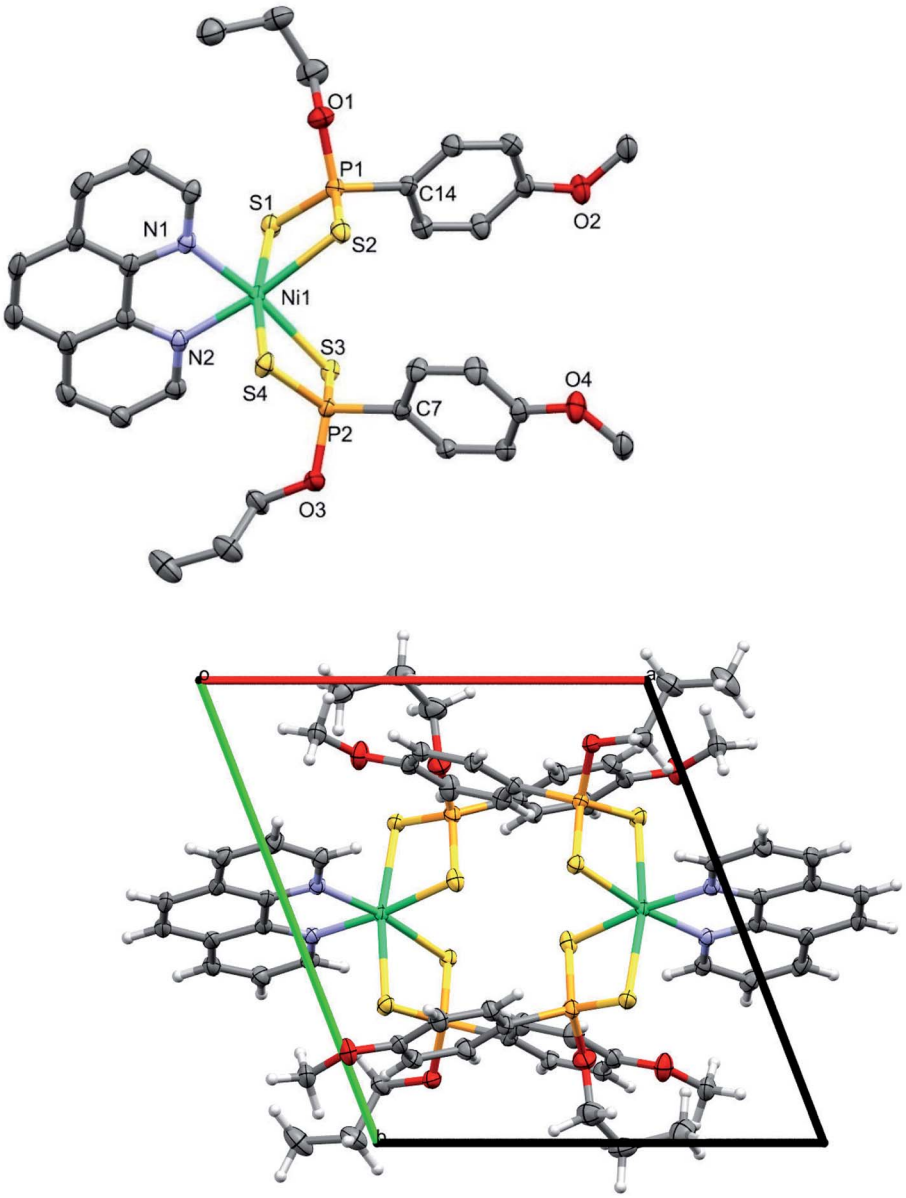

Fig. 2 Molecular representation of **2** (Thermal ellipsoids are drawn at 50% and hydrogen atoms omitted for clarity) (above) and crystal packing diagram of **2** viewed along *c*-axis (below).

refinement data are presented in Table 1. The complex is neutral and the Co center adopts a distorted octahedral geometry. Two structures of **1** were obtained (**1a** and **1b)** as polymorphs, **1a** crystallized in a monoclinic $C2/c$ space group and **1b** crystallized in a triclinic $P\bar{1}$ space group. It is a neutral 6-coordinate complex whose coordination sites include the four sulphur donor atoms of the two bidentate dithiophosphonate ligands, and two nitrogen donor atoms of 1,10-phenanthroline. The bond angles for S–Co–S average at 86° and N–Co–N average at 76°. The bond angles are smaller than 90°, typically expected for ideal octahedral complexes due to restricted intraligand bite. The bond distances for Co–S, Co–N and P–S range from 2.457(5)–2.5496(5) Å, 2.1473(14)–2.1526(9) Å and 1.9898(6)–1.9992(4) Å, respectively. The intraligand S···S bite average at 3.326 Å. The crystal structure for **1** is shown in Fig. 1 and selected bond lengths (Å) and angles (°) for **1a** and **1b** are shown in Table 2.

The Ni(II) complex, **2** crystallized in a triclinic space group $P\bar{1}$ and its crystallographic data are listed in Table 1. The complex is neutral, mononuclear and 6-coordinate with a distorted octahedral geometry around the Ni(II) center stabilized by four S donor atoms from two bidentate dithiophosphonate ligands and two N donor atoms from the 1,10-phenanthroline, shown in Fig. 2. The Ni–S distances are in the range 2.3034(4) - 2.3451(4) Å, which are in good agreement with previous reports.[52] The Ni–N bond distances range from 2.1336(13) - 2.0588(15) Å and the P–S bonds average at 2.028 Å. The S–Ni–S bond angles average at 87° and the N–Ni–N bond angles average at 79°, which are smaller than 90° expected for a regular octahedron due to restricted ligand bite.[52] Selected bond distances and angles are listed in Table 2.

The zinc(II) complex **3** crystallized in the triclinic space group $P\bar{1}$ and the molecular structure is shown in Fig. 3 and the crystallographic data are presented in Table 1. The crystal structure analysis revealed that **3** was a discrete mononuclear neutral species. The geometry around the zinc(II) center adopts a distorted tetrahedral configuration, coordinating through one S-donor atom from each of the two dithiophosphonate ligands in a monodentate fashion and two N-donor atoms of one 1,10-phenanthroline (bidentate) ligand in a bidentate chelating fashion. The Zn–S and Zn–N bond distances range from 2.2837(9) −2.3451(4) Å and 2.052(3) to 2.1336(3), respectively, which is within the range previously reported for a zinc(II) dithiophosphate and N-donor ligand (Zn–S: 2.285(8)- 2.3065(7) Å and Zn–N: 2.047(2) Å).[51] The P–S bond distance for the coordinated sulphur is in the range of 2.0274(6)–2.0396(13) Å and expectedly longer than the uncoordinated sulphur, which is in the range 1.9613(7)-1.9457(11) Å. The bond angles N1–Zn1–S1 and S1–Zn–S2 of the distorted tetrahedron range from 79.80(5)–120.162(15)° and is in good agreement with related reported values.[53] Selected bond distances and angles are listed in Table 3.

Table 3 Selected bond lengths (Å) and angles (°) for **3** and **4** with the estimated standard deviation (e.s.d.) in parentheses

Complex	**3**	Complex	**4**
Zn1–S1	2.3217(5)	Cd1–S1	2.6775(7)
Zn1–S2	2.3034(5)	Cd1–S2	2.6915(7)
Zn1–N1	2.1247(16)	Cd1–N1	2.374(2)
Zn1–N2	2.0588(15)	Cd1–N2	2.386(2)
S1–P1	2.0309(8)	S1–P1	1.9999(10)
S2–P2	2.0287(6)	S2–P2	1.9945(10)
S3–P1	1.9564(9)	S3–P1	2.0035(10)
S4–P2	1.9414(7)	S4–P2	1.9894(10)
P1–O1	1.6013(16)	P1–O1	1.606(2)
P2–O2	1.6125(14)	P2–O2	1.603(2)
P2–C13	1.800(2)	P2–C13	1.795(3)
O1–C3	1.443(3)	O1–C3	1.422(4)
S1–Zn1–S3	118.655(18)	S1–Cd1–S2	89.41(2)
N1–Zn–S1	114.73(4)	N1–Cd–S1	95.22(6)
N1–Zn–N2	80.26(6)	N1–Cd1–N2	70.13(8)

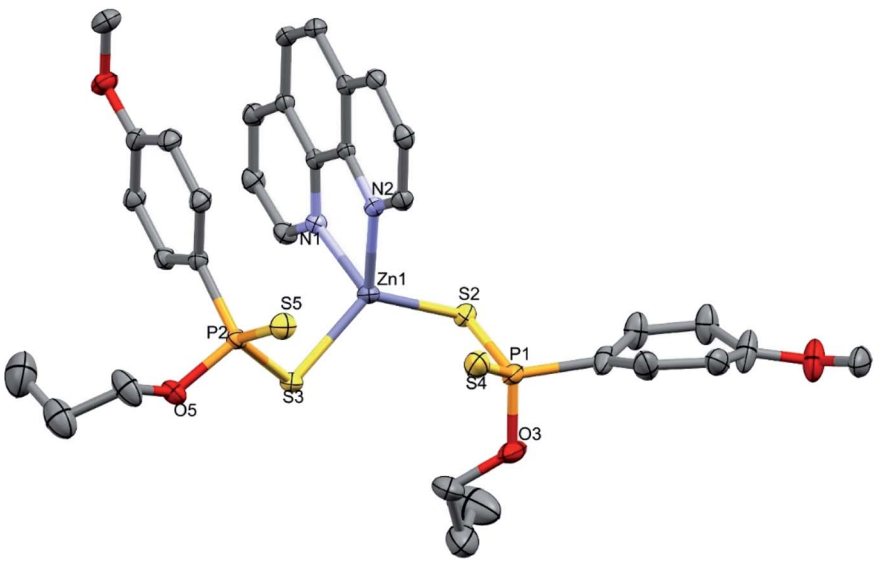

Fig. 3 Molecular structure of **3** (thermal ellipsoids are drawn at 50% and hydrogen atoms omitted for clarity).

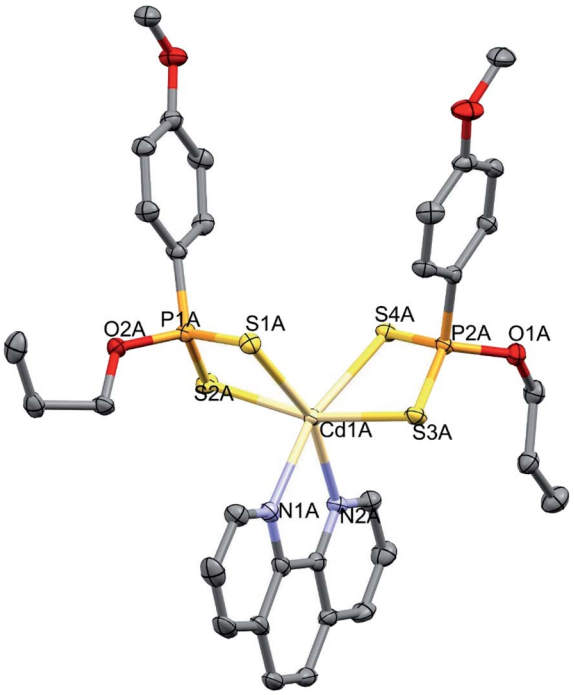

Fig. 4 Molecular structure representation of **4**. Thermal ellipsoids drawn at 50% with hydrogen atoms omitted for clarity.

Slow evaporation from acetone yielded single crystals of **4** suitable for crystallographic studies. Complex **4** crystallizes in the monoclinic space group *C*2/*c*; the unit cell consists of 2.5 symmetrically non-equivalent molecules, shown in Fig. 4. The structure of **4** revealed the first mononuclear cadmium(II) complex with this set of N and S donor ligands. The Cd(II) center adopts a distorted octahedral geometry formed by two dithiophosphonate ligands coordinating through four sulphur atoms and two N atoms of the 1,10-phenanthroline. The Cd–S distances average at 2.626 Å, which is in agreement with reported values for similar bonds reported.[54] The Cd–N bond distances average at 2.380 Å and the P–S bonds average at 1.9998 Å. The N-ligand and S-ligands are bidentate and form five and four-membered CdN_2C_2 and CdS_2P chelate rings, respectively. The S–Cd–S bond angles average at 80° and the N–Cd–N bond angles average at 70°. These angles are smaller than 90° expected for a regular octahedron due to restricted ligand bite.[54] Selected bond distances and angles are listed in Table 3.

3.4 Electrochemical studies

The molecular structures of the complexes **1–4** are summarized in Scheme 1 and for the purpose of electrochemical corrosion inhibition studies, complexes **1**, **2**, **3** and **4** are referred to as Co, Ni, Zn, and Cd, respectively.

3.4.1 Open-circuit potential (OCP) scanning. The OCP-time profile for mild steel corrosion in 1 M HCl solution in the absence and presence of 100 ppm of the studied complexes is shown in Fig. 5. The OCP *versus* time plot provides information on the stability of the electrochemical system before applying external potential or current. The obtained profile revealed that

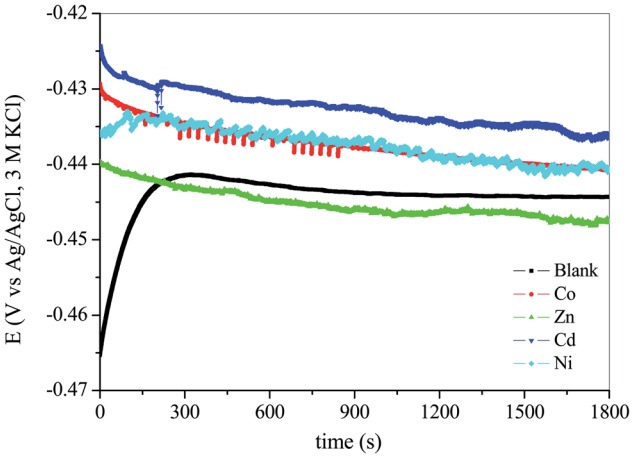

Fig. 5 OCP-time curves of mild steel in 1 M HCl without inhibitor (blank) and with 100 ppm of studied complexes at 303 K.

the system achieved a steady-state potential before the first 600 s after submerging the working electrode in the corrosive medium. The observed slight initial fluctuation of OCP can be attributed to the delayed dissolution of iron oxide layers (Fe_2O_3 and Fe_3O_4) that pose as the native protective oxide layers for the steel, and formation of defensive films by the studied complexes in the electrolytic medium.[55] At complete dissolution of the oxide layers and adsorption of studied molecules on the steel surface, the steady-state potential becomes relatively stable. The OCPs of the systems are generally stable with differentials not more than 3 mV over the entire 30 min waiting period, suggesting that the systems had assumed a sufficiently stable OCP before electrochemical perturbation.

3.4.2 Potentiodynamic polarization and linear polarization resistance (PDP and LPR). The Tafel plots obtained from the potentiodynamic polarization measurements on the working electrode in 1 M HCl in the presence and absence of 100 ppm of the studied complexes at 303 K is presented in Fig. 6. The values of electrochemical parameters such as anodic and cathodic

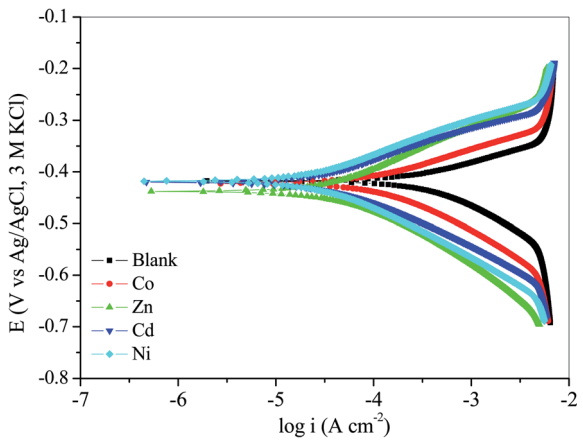

Fig. 6 Potentiodynamic polarization curves of mild steel in 1 M HCl without inhibitor (blank) and with 100 ppm of studied complexes at 303 K.

Table 4 Polarization parameters for mild steel in 1 M HCl without inhibitor (blank) and with 100 ppm of studied complexes at 303 K

	PDP					LPR	
Inhibitors	$-E_{corr}$ (mV)	i_{corr} (μA cm^{-2})	β_a (mV dec^{-1})	β_c (mV dec^{-1})	η_{PDP}	R_{PR} (Ω cm^2)	η_{LPR}
Blank	417.74	560.49	138.33	90.09	—	42.28	—
Co	422.26	153.99	112.89	83.60	72.53	135.45	68.79
Zn	438.17	49.64	102.89	107.97	91.14	460.70	90.82
Cd	420.31	43.27	91.04	96.66	92.28	470.53	91.01
Ni	418.00	32.85	99.58	90.92	94.14	628.24	93.27

Tafel slopes (β_a and β_c), corrosion current density (i_{corr}), corrosion potential (E_{corr}) and inhibition performance (η_{PDP}) are reported in Table 4. It is clear from the anodic and cathodic branches of the plots that the introduction of Co resulted in a shift to a region of lower current density as compared to the blank solution. Similar shifts were observed for the other three complexes, suggesting that all the inhibitors show similar corrosion inhibition mechanism with Ni showing the most prominent shift from the blank. This observation suggests that the four studied complexes impede steel corrosion by forming an inhibitive film at the active sites on the metallic surface.[41,56]

The mode of corrosion inhibition exhibited by Co, Zn, Cd and Ni can be classified as anodic, cathodic or mixed-type based on the magnitude of displacement of their E_{corr} compared to that of the blank. It is generally reported that a shift in E_{corr} value less than 85 mV describes a mixed-type inhibitor while a shift in E_{corr} greater than 85 mV is categorized as cathodic or anodic.[57,58] In the present study, the maximum displacement in E_{corr} ranged from 0.26 to 20.43 mV, which proposes that the studied compounds are mixed-type corrosion inhibitors. In other words, the studied inhibitors exhibited the ability to simultaneously restrain anodic dissolution of mild steel and cathodic evolution of hydrogen gas. The obtained values of the Tafel slopes showed a small deviation on the addition of the inhibitors as compared to the blank solution, which suggests that the adsorption mechanism is unaffected by the addition of the inhibitors. The studied inhibitors simply adsorb on the metal surface and block the active sites.[50] This was further substantiated by the changes in the values of the anodic and cathodic slopes for the inhibited systems. Factors under consideration when discussing the efficiency of corrosion inhibitors include the presence of heteroatoms, molecular size,

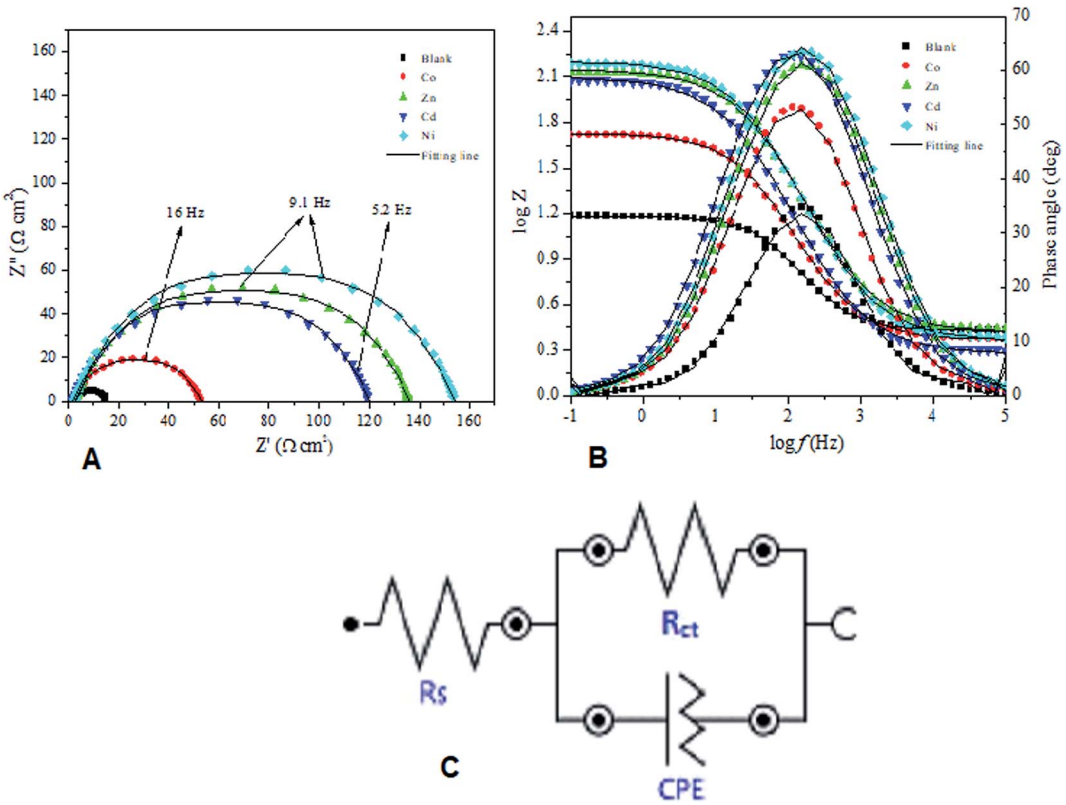

Fig. 7 (a–c). Nyquist plot (A), Bode plot (B) and Randle equivalent circuit (C) for mild steel in 1 M HCl without inhibitor (blank) and with 100 ppm of complexes studied at 303 K.

Table 5 Electrochemical impedance spectroscopy parameters obtained for studied compounds at 303 K

Inhibitor	R_s (Ω cm^2)	R_{ct} (Ω cm^2)	n	Y_0 ($\mu\Omega$ s^n cm^{-2})	$-\alpha$	$-S$	C_{dl} (μF cm^{-2})	χ^2	η_{EIS}
Blank	2.69	12.5	0.835	613.0	34.86	0.41	234.10	0.18807	—
Co	2.37	50.4	0.835	361.0	53.16	0.56	163.56	0.24371	75.20
Zn	1.98	118.0	0.853	235.0	60.91	0.69	126.69	0.33546	89.41
Cd	2.73	133.0	0.845	151.0	62.95	0.64	73.73	0.31865	90.60
Ni	2.42	152.0	0.856	141.0	63.48	0.71	73.87	0.35772	91.78

molecular geometry, electron charge density, mode of interaction, number of functional groups, and so on.[56–58] The large molecular size, molecular geometry and the presence of donor atoms such as N, O, S and P in the studied complexes might contribute to their excellent inhibition properties. The order of inhibition efficiencies is Ni (94.14%) > Cd (92.28%) > Zn (91.14%) > Co (72.53%). The observed higher inhibition efficiency for Ni follows the trend previously reported.[59,60] Furthermore, electrochemical parameters obtained from linear polarization measurements revealed that the studied complexes behaved as excellent corrosion inhibitors for mild steel in the studied acidic medium. The values of polarization resistance (R_p) which are obtained from the slope of current density–potential graph for each studied complex ranged from 135.45 to 628.24 Ω cm^2 and were greater than the 42.28 Ω cm^2 of the uninhibited solution. This suggests that the adsorbed portions of the complex on the steel surface have successfully blocked the active sites and inhibited dissolution of the metal.

3.4.3 Electrochemical impedance spectroscopy (EIS). EIS was employed as a reliable method for gaining better insight into the behaviour of mild steel–inhibitor interfaces. The Nyquist and Bode plots for steel corrosion in the corrosive medium in the absence and presence of 100 ppm Co, Zn, Cd and Ni at 303 K are shown in Fig. 7a and b. The Nyquist plots of the uninhibited and additive-containing media (with the studied complexes) revealed depressed semicircles indicating the mechanism of steel corrosion was the same in all cases. Careful interpretation of the impedance spectra showed that the introduction of 100 ppm of different complexes resulted in a significant increase in the size of the semicircles and the charge transfer resistance. This indicated that the studied complexes adsorbed on the surface of the metal specimen, thereby forming a protective layer on the mild surface.[39,61] A simple Randle circuit (equivalent circuit) comprising a constant phase element (CPE), solution resistance (R_s) and charge transfer resistance (R_{ct}) shown in Fig. 7c employed to fit the impedance spectra showed excellent fitting with the goodness of fit values ranging from 0.18807 to 0.35772. The EIS parameters derived from the spectra are presented in Table 5.

The tabulated results (Table 5) showed an increase in the values of R_{ct} from 12.5 Ω cm^2 (for the blank solution) to values ranging from 50.4 to 152.0 Ω cm^2 with the introduction of 100 ppm of Co, Ni, Cd and Zn complexes, which correspond to the ability of the complexes to impede charge transfer across steel/electrolyte interface. An inhibition efficiency of 91.78% was recorded at 100 ppm of Ni complex at 303 K. Additionally, a drop was observed in the values of C_{dl} with the introduction of the complexes. The significant increase in the R_{ct} values is due to the formation of a shielding layer on the mild steel surface by the inhibitor molecules.[58] The observed decrease in C_{dl} can be correlated to the thickness of the protective layer on the steel/acid interface, which is attributed to gradual replacement of water molecules by the inhibitor molecules.[62] The double-layer capacitance (C_{dl}) for mild steel corrosion in the acid and in the presence of the inhibitors was calculated using the equation:[50]

$$C_{dl} = (Y_o R_{ct}^{1-n})^{1/n}$$

where Y_0 is the CPE constant, R_{ct} represents the charge-transfer resistance and n (a CPE exponent) is the phase shift which is often used to categorize the nature of the CPE, and also as a measure of the degree of roughness of the electrode surface.[50] A unit value of n characterizes the CPE to be purely capacitive, while near unity values have been associated with pseudocapacitive electrode surface. The values of n obtained from the EIS as listed in Table 5 are near unity, suggesting the pseudocapacitive behaviour of the electrode surface. Moreover, the values of n in the presence of inhibitors are slightly higher than that for the inhibitor-free medium (except for Co), suggesting that the steel surface assumes less inhomogeneity in the inhibitor-containing solutions, due to uniform coverage of the electrode surface by the adsorbed inhibitor molecules.[50]

Furthermore, the Bode diagram (Fig. 7b) for the steel corrosion in the presence and absence of the studied complexes features a one-phase peak which confirms that the corrosion process exhibited a single time-constant and is mainly controlled by a single charge transfer mechanism.[61]

The values of the phase angles (α) and slopes (S) obtained from the linear portion of the Bode plot at the middle frequency range are recorded in Table 5. The observed trend of increase in the value of the phase angle on introducing the studied complexes to the blank solution indicate the formation of a protective film on the mild steel surface. In addition, the obtained $-\alpha$ and $-S$ which ranged from 53.16–63.48 and 0.56–0.71 respectively for the studied complexes suggest that the electrode/electrolyte interface acts a pseudocapacitor where an ideal capacitor has a α of -90 and S of -1.[63,64] The computed inhibition potentials from the different electrochemical methods employed in the study showed excellent agreement.

3.5 Computational study

3.5.1 Quantum chemical descriptor calculations. Quantum chemical descriptors of the four metal complexes (Co, Ni, Zn, and Cd) were investigated to correlate their electronic structures

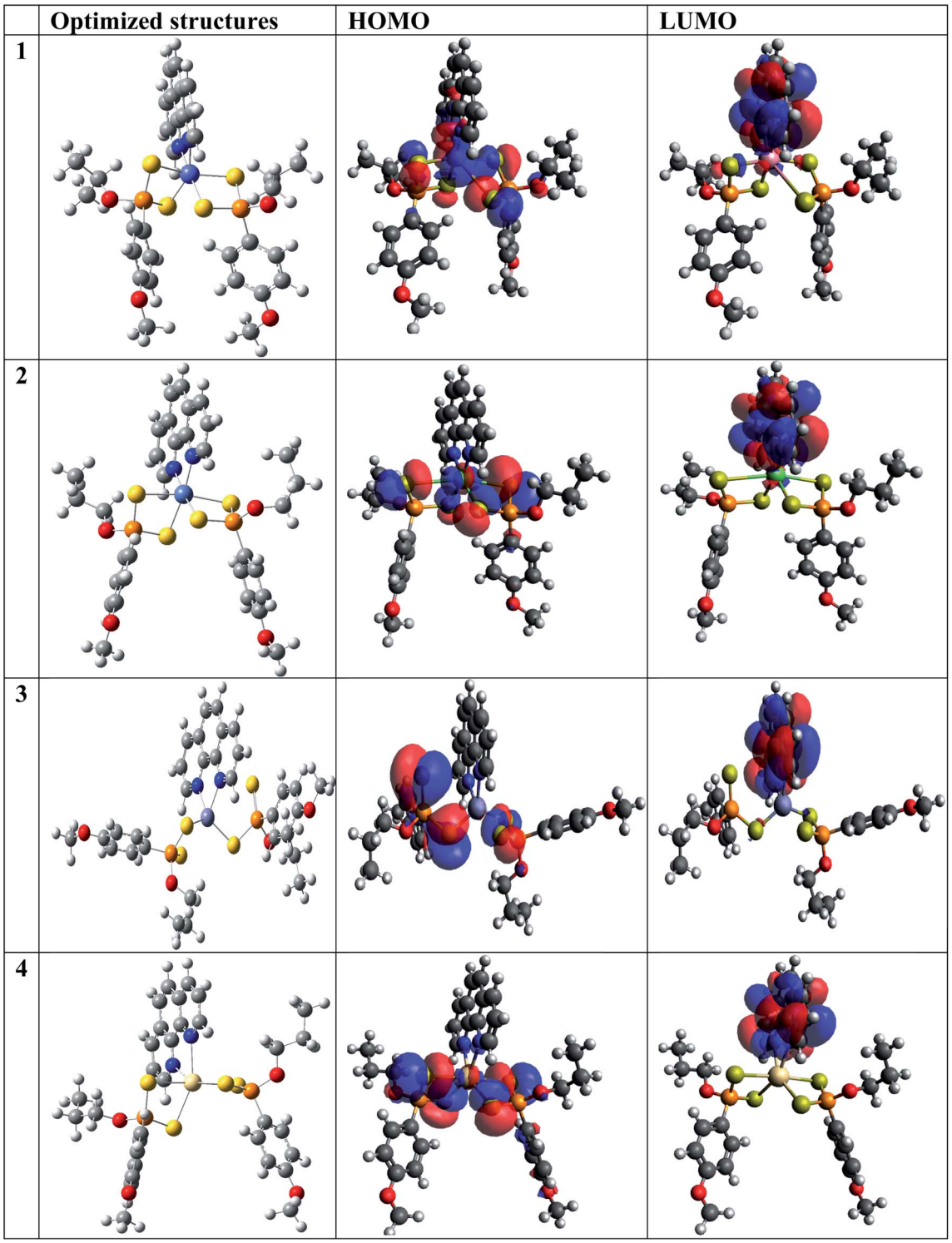

Fig. 8 The optimized structures and HOMO and LUMO electron density isosurfaces of Co, Zn, Cd and Ni complexes at BP86/Def2TZVP and B3LYP/LANL2DZ levels.

to their reactivities and viz-a-viz performances as corrosion inhibitors.[65] The structures of the metal complexes were optimized using BP86 method with Def2TZVP for Zn, Co and Cd complexes while B3LYP with LANL2DZ basis set for Ni. The optimized structures, highest occupied molecular orbitals (HOMO) and lowest unoccupied molecular orbitals (LUMO) electron density isosurfaces for the studied metal complexes are shown in Fig. 8.

The HOMO and LUMO electron density isosurfaces of all the metal complexes showed similar delocalization patterns. The

Table 6 The calculated quantum chemical parameters for the metal complexes using BP86/Def2TZVP and B3LYP/LANL2DZ levels

Parameters	Co	Zn	Cd	Ni
E_{HOMO}	−4.099	−4.751	−4.691	−5.096
E_{LUMO}	−2.99	−3.293	−3.156	−2.744
ΔE	1.109	1.458	1.535	2.352
η (eV)	0.5545	0.729	0.7675	0.4252
S (eV^{-1})	0.9017	0.6859	0.6515	0.4255
I (eV)	4.099	4.751	4.691	5.096
A (eV)	2.99	3.293	3.156	2.774
χ (eV)	−3.6275	−4.022	−3.9235	−3.92
ω (eV)	11.8654	11.095	10.0285	6.533
μ (debye)	4.5615	8.2503	5.4076	5.9329

HOMOs were localized on the central metal atom coordinated with highly electronegative atoms such as S, O and P in all cases while the LUMOs are delocalized on the 1,10-phenanthroline aromatic rings. Similar observations have been previously reported.[66]

The obtained quantum chemical parameters such as the E_{HOMO}, E_{LUMO}, ΔE, η, S, A, I, χ, μ and ω for the studied metal complexes are shown in Table 6. The energy of the HOMOs (E_{HOMO}) was higher indicating its ability to release electrons from the metal to be accepted by the LUMOs having lower energy (E_{LUMO}). Co has the lowest energy gap (1.109 eV), that is, it is more reactive than Zn, Cd and Ni. The energy gap of Co corresponds to its higher value of softness showing the greater tendency to donate an electron to the metal surface. As reported in Table 6, the electrophilicity value of the Co metal complex was higher than Zn, Cd and Ni, this supported the observation that Co complex is most reactive. The theoretical and experimental results are in good agreement except for Co^{2+} which showed the least inhibition property thereby contradicting the experimental. The tendency of Co^{2+} to oxidize to Co^{3+} in the presence of HCl (a strong oxidizing agent) accounts for why the theoretical results deviates from the experimental results presented. It, therefore, implies that Co^{2+} was partially oxidized in HCl solution.

4. Conclusions

Heteroleptic complexes of four divalent metals, Co, Ni, Zn, and Cd with dithiophosphonates and N-donor ligands were successfully synthesized and fully characterized by FT-IR, magnetic moment measurements, elemental analysis and mass spectrometry. Structural elucidation of all the four complexes was achieved by single-crystal X-ray studies. The crystal structures revealed the first known Co^{2+} complexes of dithiophosphonates, as well as first mononuclear 4-coordinate zinc complexes. The metal complexes showed excellent corrosion inhibition potentials for mild steel in 1 M HCl. The complexes gave inhibition efficiencies of 75.20% (Co), 89.41% (Zn), 90.60% (Cd) and 91.78% (Ni) when applied at 100 ppm to mild steel in 1 M HCl.

Conflicts of interest

The authors declare no conflict of interest.

Acknowledgements

TLY acknowledge UKZN for providing research infrastructure.

References

1 D. de la Fuente, I. Diaz, J. Simancas, B. Chico and M. Morcillo, Long-term Atmospheric Corrosion of Mild Steel, *Corros. Sci.*, 2011, **53**, 604, DOI: 10.1016/j.corsci.2010.10.007.

2 B. Chugh, A. K. Singh, S. Thakur, B. Pani, A. K. Pandey, H. Lgaz, I.-M. Chung and E. E. Ebenso, An Exploration about the Interaction of Mild Steel with Hydrochloric Acid in the Presence of *N*-(Benzo[*d*]thiazole-2-yl)-1-phenylethan-1-imine, *J. Phys. Chem. C*, 2019, **123**, 22897–22917.

3 D. K. Singh, S. Kumar, G. Udayabhanu and R. P. John, 4(*N*,*N*-Dimethylamino)benzaldehyde nicotinic hydrazone as corrosion inhibitor for mild steel in 1 M HCl solution: an experimental and theoretical study, *J. Mol. Liq.*, 2016, **216**, 738–746, DOI: 10.1016/j.molliq.2016.02.012.

4 A. Gajek, T. Zakroczymski, V. Romanchuk and P. Topilnytsky, Protective Properties and Spectral Analysis of Nitrogen- and Oxygen-Containing Corrosion Inhibitors for Oil Equipment, *Chem. Chem. Technol.*, 2012, **6**, 209, DOI: 10.23939/chcht06.02.209.

5 S. Pinchuk, S. Gubenko and E. Belaya, Correlation between Electrochemical Corrosion and Structural State of Steel by Simulation of Operation Conditions of Railway Wheels, *Chem. Chem. Technol.*, 2010, **4**, 151.

6 K. K. Alaneme, S. J. Olusegun and O. T. Adelowo, Corrosion inhibition and adsorption mechanism studies of *Hunteria umbellata* seed husk extracts on mild steel immersed in acidic solutions, *Alexandria Eng. J.*, 2016, **55**, 673–681, DOI: 10.1016/j.aej.2015.10.009.

7 X. Luo, C. Ci, J. Li, K. Lin, S. Du, H. Zhang, X. Li, Y. F. Cheng, J. Zang and Y. Liu, 4-Aminoazobenzene modified natural glucomannan as a green eco-friendly inhibitor for the mild steel in 0.5 M HCl solution, *Corros. Sci.*, 2019, **151**, 132–142, DOI: 10.1016/j.corsci.2019.02.027.

8 F. Bentiss, M. Lagrenee, M. Traisnel and J. Hornez, The corrosion inhibition of mild steel in acidic media by a new triazole derivative, *Corros. Sci.*, 1999, **41**, 789–803, DOI: 10.1016/S0010-938X(98)00153-X.

9 (*a*) A. K. Singh and M. Quraishi, Effect of Cefazolin on the Corrosion of Mild Steel in HCl Solution, *Corros. Sci.*, 2010, **52**, 152–160; (*b*) A. R. Sayed, M. M. Saleh, M. A. Al-Omair and H. M. Abd Al-Lateef, Efficient route synthesis of new polythiazoles and their inhibition characteristics of mild-steel corrosion in acidic chloride medium, *J. Mol. Struct.*, 2019, **1184**, 452–461, DOI: 10.1016/j.molstruc.2019.02.061.

10 F. E.-T. Heakal and A. E. Elkholy, Gemini surfactants as corrosion inhibitors for carbon steel, *J. Mol. Liq.*, 2017, **230**, 395–407, DOI: 10.1016/j.molliq.2017.01.047.

11 K. F. Khaled, New Synthesized Guanidine Derivative as a Green Corrosion Inhibitor for Mild Steel in Acidic Solutions, *Int. J. Electrochem. Sci.*, 2008, **3**, 462.

12 M. Lebrini, A. Lagrenee, A. Traisnel, L. Gengembre, H. Vezin and F. Bentiss, Enhanced Corrosion Resistance of Mild Steel in Normal Sulfuric Acid Medium by 2,5-bis(n-thienyl)-1,3,4-thiadiazoles: Electrochemical, X-ray Photoelectron Spectroscopy and Theoretical Studies, *Appl. Surf. Sci.*, 2007, **253**, 9267, DOI: 10.1016/j.apsusc.2007.05.062.

13 D. Guzman-Lucero, O. Olivares-Xometl, R. Martinez-Palou, N. V. Likhanova, M. A. Dominguez-Aguilar and V. Garibay-Febles, Synthesis of Selected Vinylimidazolium Ionic Liquids and their Effectiveness as Corrosion Inhibitors for Carbon Steel in Aqueous Sulfuric Acid, *Ind. Eng. Chem. Res.*, 2011, **50**, 7129, DOI: 10.1021/ie1024744.

14 E. E. Ebenso, T. Arslan, F. Kandemirli, I. Love, C. O. Gretir, M. Saracoglu and S. A. Umoren, Theoretical Studies of Some Sulphonamides as Corrosion Inhibitors for Mild Steel in Acidic Medium, *Int. J. Quantum Chem.*, 2010, **110**, 2614, DOI: 10.1002/qua.22430.

15 A. Popova, M. Christov and A. Zwetanova, Effect of the molecular structure on the inhibitor properties of azoles on mild steel corrosion in 1 M hydrochloric acid, *Corros. Sci.*, 2007, **49**, 2131–2143, DOI: 10.1016/j.corsci.2006.10.021.

16 (*a*) B. Chugh, A. K. Singh, D. Poddar, S. Thakur, B. Pani and P. Jain, Relation of degree of substitution and metal protecting ability of cinnamaldehyde modified chitosan, *Carbohydr. Polym.*, 2020, **234**, 115945; (*b*) F. Bentiss, M. Lebrini and M. Lagrenée, Thermodynamic characterization of metal dissolution and inhibitor adsorption processes in mild steel/2,5-bis(*n*-thienyl)-1,3,4-thiadiazoles/hydrochloric acid system, *Corros. Sci.*, 2005, **47**, 2915–2931, DOI: 10.1016/j.corsci.2005.05.034.

17 K. Bhrara, H. Kim and G. Singh, Inhibiting effects of butyl triphenyl phosphonium bromide on corrosion of mild steel in 0.5 M sulphuric acid solution and its adsorption characteristics, *Corros. Sci.*, 2008, **50**, 2747–2754, DOI: 10.1016/j.corsci.2008.06.054.

18 (*a*) A. K. Singh, S. Thakur, B. Pani and G. Singh, Green synthesis and corrosion inhibition study of 2-amino-*N*′-((thiophen-2-yl)methylene)benzohydrazide, *New J. Chem.*, 2018, **42**, 2113–2124; (*b*) S. K. Ahmed, W. B. Ali and A. A. Khadom, Synthesis and investigations of heterocyclic compounds as corrosion inhibitors for mild steel in hydrochloric acid, *Int. J. Ind. Chem.*, 2019, **10**, 159–173, DOI: 10.1007/s40090-019-0181-8.

19 M. A. Quraishi, 2-Amino-3,5-dicarbonitrile-6-thio-pyridines: new and effective corrosion inhibitors for mild steel in 1 M HCl, *Ind. Eng. Chem. Res.*, 2014, **53**, 2851–2859, DOI: 10.1021/ie401633y.

20 A. Y. Musa, A. A. H. Kadhum, A. B. Mohamad and M. S. Takriff, Experimental and theoretical study on the inhibition performance of triazole compounds for mild steel corrosion, *Corros. Sci.*, 2010, **52**, 3331–3340, DOI: 10.1016/j.corsci.2010.06.002.

21 V. P. Singh, P. Singh and A. K. Singh, Synthesis, structural and corrosion inhibition studies on cobalt(II), nickel(II), copper(II) and zinc(II) complexes with 2-acetylthiophene benzoylhydrazone, *Inorg. Chim. Acta*, 2011, **379**, 56–63, DOI: 10.1016/j.ica.2011.09.037.

22 M. Mahdavian and M. Attar, Electrochemical behaviour of some transition metal acetylacetonate complexes as corrosion inhibitors for mild steel, *Corros. Sci.*, 2009, **51**, 409–414, DOI: 10.1016/j.corsci.2008.11.010.

23 Z. Ahmad, *Principles of corrosion engineering and corrosion control*, Elsevier, 2006.

24 M. Attar, Investigation on zinc phosphate effectiveness at different pigment volume concentrations *via* electrochemical impedance spectroscopy, *Electrochim. Acta*, 2005, **50**, 4645–4648, DOI: 10.1016/j.electacta.2005.02.015.

25 F. Mansfeld, M. Kendig and S. Tsai, Evaluation of corrosion behavior of coated metals with AC impedance measurements, *Corrosion*, 1982, **38**, 478–485, DOI: 10.5006/1.3577363.

26 M. Mahdavian and M. Attar, Evaluation of zinc phosphate and zinc chromate effectiveness *via* AC and DC methods, *Prog. Org. Coat.*, 2005, **53**, 191–194, DOI: 10.1016/j.porgcoat.2005.02.007.

27 J. R. MacDonald, *Impedance Spectroscopy–Emphasizing Solid Materials and Systems*, Wiley-Interscience, John Wiley and Sons, 1987, pp. 1–346.

28 L. O. Olasunkanmi, I. B. Obot, M. M. Kabanda and E. E. Ebenso, Some Quinoxalin-6-yl Derivatives as Corrosion Inhibitors for Mild Steel in Hydrochloric Acid: Experimental and Theoretical Studies, *J. Phys. Chem. C*, 2015, **119**, 16004–16019, DOI: 10.1021/acs.jpcc.5b03285.

29 I. B. Obot and N. O. Obi-Egbedi, Indeno-1-one-[2,3-*b*]-quinoxaline as an Effective Inhibitor for the Corrosion of Mild Steel in 0.5 M H_2SO_4 Solution, *Mater. Chem. Phys.*, 2010, **122**, 325, DOI: 10.1016/j.matchemphys.2010.03.037.

30 I. El Ouali, B. Hammouti, A. Aouniti, Y. Ramli, M. Azougagh, E. M. Essassi and M. Bouachrine, Thermodynamic Characterisation of Steel Corrosion in HCl in the Presence of 2-phenylthieno-(3,2-*b*)-quinoxaline, *J. Mater. Environ. Sci.*, 2010, **1**, 1.

31 J. J. Fu, H. S. Zang, Y. Wang, S. N. Li, T. Chen and X. D. Liu, Experimental and Theoretical Study on the Inhibition Performances of Quinoxaline and Its Derivatives for the Corrosion of Mild Steel in Hydrochloric Acid, *Ind. Eng. Chem. Res.*, 2012, **51**, 6377, DOI: 10.1021/ie202832e.

32 A. M. Barnes, K. D. Bartle and V. R. A. Thibon, A review of zinc dialkyldithiophosphates (ZDDPS): characterisation and role in the lubricating oil, *Tribol. Int.*, 2001, **34**, 389–395, DOI: 10.1016/S0301-679X(01)00028-7.

33 *Bruker, APEXII*, APEXII Bruker AXS Inc, Madison, Wisconsin, USA, 2009.

34 . *Bruker, SAINT*, SAINT Bruker AXS InC, Madison, Wisconsin, USA, 2009.

35 *Bruker, SADABS*, SADABS Bruker AXS Inc, Madison, Wisconsin, USA, 2009.

36 G. M. Sheldrick, A short history of SHELX, *Acta Crystallogr., Sect. A: Found. Crystallogr.*, 2008, **64**, 112–122.

37 C. F. Macrae, I. J. Bruno, J. A. Chisholm, P. R. Edgington, P. McCabe, E. Pidcock, L. Rodriguez-Monge, R. Taylor, J. Streek and P. A. Wood, Mercury CSD 2.0–new features for the visualization and investigation of crystal structures,

J. Appl. Crystallogr., 2008, **41**, 466–470, DOI: 10.1107/S0021889807067908.

38 (*a*) ASTM International, *American Society for Testing and Materials - ASTM G106-89: Standard Practice for Verification of Algorithm and Equipment for Electrochemical Impedance Measurements*. Reapproved, 1999; (*b*) B. J. E. Merten, *Electrochemical Impedance Methods to Assess Coatings for Corrosion Protection*, Technical Service Center, Materials and Corrosion Laboratory, U.S. Department of the Interior, Bureau of Reclamation, PO Box 25007, Denver CO 80225-0007, 2019.

39 E. D. Akpan, I. O. Isaac, L. O. Olasunkanmi, E. E. Ebenso and E.-S. M. Sherif, Acridine-based thiosemicarbazones as novel inhibitors of mild steel corrosion in 1 M HCl: synthesis, electrochemical, DFT and Monte Carlo simulation studies, *RSC Adv.*, 2019, **9**, 29590–29599, DOI: 10.1039/C9RA04778F.

40 ASTM International, *American Society for Testing and Materials – ASTM F 2129-01 "Standard Test Method for Conducting Cyclic Potentiodynamic Polarization Measurements to Determine the Corrosion Susceptibility of Small Implant Devices"*, West Conshohocken, PA, 2001.

41 K. Zakaria, N. A. Negm, E. A. Khamis and E. A. Badr, Electrochemical and quantum chemical studies on carbon steel corrosion protection in 1 M H_2SO_4 using new eco-friendly Schiff base metal complexes, *J. Taiwan Inst. Chem. Eng.*, 2016, **61**, 316–326, DOI: 10.1016/j.jtice.2015.12.021.

42 A. Aytaç, Cu(II), Co(II) and Ni(II) complexes of –Br and $-OCH_2CH_3$ substituted Schiff bases as corrosion inhibitors for aluminium in acidic media, *J. Mater. Sci.*, 2010, **45**, 6812–6818, DOI: 10.1007/s10853-010-4779-7.

43 M. K. Assefa, J. L. Devera, A. D. Brathwaite, J. D. Mosley and M. A. Duncan, Vibrational scaling factors for transition metal carbonyls, *Chem. Phys. Lett.*, 2015, **640**, 175–179, DOI: 10.1016/j.cplett.2015.10.031.

44 M. Robb, *New Chemistry with Gaussian 16 & GaussView 6*.

45 C. W. Liu, Y. R. Lin, C. S. Fang, C. Latouche, S. Kahlal and J. Y. Saillard, $[Ag_7(H)\{E_2P(OR)_2\}_6]$ (E = Se, S): precursors for the fabrication of silver nanoparticles, *Inorg. Chem.*, 2013, **52**, 2070–2077, DOI: 10.1021/ic302482p.

46 A. D. Becke, A new mixing of Hartree–Fock and local density-functional theories, *J. Chem. Phys.*, 1993, **98**, 1372–1377, DOI: 10.1063/1.464304.

47 S. Banerjee, D. Sheet, S. Sarkar, P. Halder and T. K. Paine, Nickel complexes of ligands derived from (*o*-hydroxyphenyl) dichalcogenide: delocalised redox states of nickel and *o*-chalcogenophenolate ligands, *Dalton Trans.*, 2019, **48**, 17355–17363, DOI: 10.1039/C9DT03413G.

48 X. Li and M. J. Frisch, Energy-Represented Direct Inversion in the Iterative Subspace within a Hybrid Geometry Optimization Method, *J. Chem. Theory Comput.*, 2006, **2**, 835–839, DOI: 10.1021/ct050275a.

49 J. C. Phillips, Generalized Koopmans' Theorem, *Phys. Rev.*, 1961, **123**, 420–424, DOI: 10.1103/PhysRev.123.420.

50 P. Singh, D. P. Singh, K. Tiwari, M. Mishra, A. K. Singh and V. P. Singh, Synthesis, structural investigations and corrosion inhibition studies on Mn(II), Co(II), Ni(II), Cu(II) and Zn(II) complexes with 2-amino-benzoic acid (phenyl-pyridin-2-yl-methylene)-hydrazide, *RSC Adv.*, 2015, **5**, 45217–45230, DOI: 10.1039/C4RA11929K.

51 L. Glinskaya, V. Shchukin, R. Klevtsova, A. Mazhara and S. Larionov, Synthesis and polymer structure of [Zn (4,4′-bipy)$\{(^iPrO)_2PS_2\}_2]_n$ and thermal properties of ZnL $\{(i\text{-}PrO)_2PS_2\}_2$ (L = phen, 2,2′-bipy, 4,4′-bipy), *J. Struct. Chem.*, 2000, **41**, 632–639, DOI: 10.1007/BF02683926.

52 E. G. Sağlam, C. T. Zeyrek, H. Dal, H. Ünver and A. Ebinç, New {bis-pyridine-bis-[3-methyl-1-butoxy-(*p*-methoxyphenyl) phosphonodithioato]}nickel(II) complex: Synthesis, characterization, single crystal structure and theoretical studies, *J. Mol. Struct.*, 2020, **1201**, 127185, DOI: 10.1016/j.molstruc.2019.127185.

53 L. Jeremias, G. Demo, M. Babiak, J. Vícha, Z. Trávníček and J. Novosad, X-ray structures of heteroleptic zinc (II) complexes involving combinations of O, O′-dialkyldithiophosphato and bidentate N-donor ligands, *Z. Kristallogr. - Cryst. Mater.*, 2014, **229**, 537–542, DOI: 10.1515/zkri-2014-1736.

54 A. Banaei, A. Saadat, M. Mohammad Goli, P. McArdle, E. Pourbasheer and P. Pargolghasemi, Synthesis, characterization, and molecular structures of Ni(II) and Cd(II) complexes derived from dithiophosphonate, *Heteroat. Chem.*, 2016, **27**, 353–360, DOI: 10.1002/hc.21345.

55 S. Kumari, H. R. Tiyyagura, T. E. L. Douglas, E. A. A. Mohammed, A. Adriaens, R. Fuchs-Godec, M. K. Mohan and A. G. Skirtach, ANN prediction of corrosion behaviour of uncoated and biopolymers coated cp-Titanium substrates, *Mater. Des.*, 2018, **157**, 35–51, DOI: 10.1016/j.matdes.2018.07.005.

56 R. R. Arvizo, S. Bhattacharyya, R. A. Kudgus, K. Giri, R. Bhattacharya and P. Mukherjee, Intrinsic therapeutic applications of noble metal nanoparticles: past, present and future, *Chem. Soc. Rev.*, 2012, **41**, 2943–2970, DOI: 10.1039/c2cs15355f.

57 H. Tayebi, H. Bourazmi, B. Himmi, A. El Assyry, Y. Ramli, A. Zarrouk, A. Geunbour, B. Hammouti and E. E. Ebenso, An electrochemical and theoretical evaluation of new quinoline derivative as a corrosion inhibitor for carbon steel in HCl solutions, *Der Pharm. Lett.*, 2014, **6**, 20–34.

58 H. Lgaz, R. Salghi, K. Subrahmanya Bhat, A. Chaouiki, Shubhalaxmi and S. Jodeh, Correlated experimental and theoretical study on inhibition behavior of novel quinoline derivatives for the corrosion of mild steel in hydrochloric acid solution, *J. Mol. Liq.*, 2017, **244**, 154–168, DOI: 10.1016/j.molliq.2017.08.121.

59 S. Kashyap, S. Kumar, K. Ramasamy, S. M. Lim, S. A. A. Shah, H. Om and B. Narasimhan, Synthesis, biological evaluation and corrosion inhibition studies of transition metal complexes of Schiff base, *Chem. Cent. J.*, 2018, **12**, 1–10, DOI: 10.1186/s13065-018-0487-1.

60 M. Mishra, K. Tiwari, P. Mourya, M. M. Singh and V. P. Singh, Synthesis, characterization and corrosion inhibition property of nickel(II) and copper(II) complexes with some acylhydrazine Schiff bases, *Polyhedron*, 2015, **89**, 29–38, DOI: 10.1016/j.poly.2015.01.003.

61 A. S. Fouda, M. A. Ismail, A. M. Temraz and A. S. Abousalem, Comprehensive investigations on the action of cationic terthiophene and bithiophene as corrosion inhibitors: experimental and theoretical studies, *New J. Chem.*, 2019, **43**, 768–789, DOI: 10.1039/C8NJ04330B.

62 S. M. Tawfik and M. F. Zaky, Corrosion inhibition performance of some Schiff base anionic surfactant complexes of cobalt(II), copper(II), and zinc(II) on carbon steel in 1.0 M HCl, *Res. Chem. Intermed.*, 2015, **41**, 8747–8772, DOI: 10.1007/s11164-015-1926-4.

63 L. O. Olasunkanmi, M. M. Kabanda and E. E. Ebenso, Quinoxaline derivatives as corrosion inhibitors for mild steel in hydrochloric acid medium: electrochemical and quantum chemical studies, *Phys. E*, 2016, **76**, 109–126, DOI: 10.1016/j.physe.2015.10.005.

64 C. Verma, L. O. Olasunkanmi, T. W. Quadri, El-S. M. Sherif and E. E. Ebenso, Gravimetric, electrochemical, surface morphology, DFT, and Monte Carlo simulation studies on three N-substituted 2-aminopyridine derivatives as corrosion inhibitors of mild steel in acidic medium, *J. Phys. Chem. C*, 2018, **122**, 11870–11882, DOI: 10.1021/acs.jpcc.5b03285.

65 B. E. Brycki, I. H. Kowalczyk, A. Szulc, O. Karczewska, M. Pakiet and M. Aliofkhazraei, InTech Open, in *Corrosion Inhibitors, Principles and Recent Applications*, 2017, vol. 72943, pp. 21–22. DOI: 10.5772/intechopen.

66 A. C. Ekennia, D. C. Onwudiwe, A. A. Osowole, L. O. Olasunkanmi and E. E. Ebenso, Synthesis, Biological, and Quantum Chemical Studies of Zn(II) and Ni(II) Mixed-Ligand Complexes Derived from *N*,*N*-Disubstituted Dithiocarbamate and Benzoic Acid, *J. Chem.*, 2016, **2016**, 5129010, DOI: 10.1155/2016/5129010.

